


Cite this: *RSC Adv.*, 2022, 12, 4029

# Hexadecyl trimethyl ammonium bromide assisted growth of $\text{NiCo}_2\text{O}_4$ @reduced graphene oxide/nickel foam nanoneedle arrays with enhanced performance for supercapacitor electrodes†

Tingting Liu,<sup>\*a</sup> Shuai Zhou,<sup>b</sup> Xuehan Yu,<sup>b</sup> Chao Mao,<sup>b</sup> Yujie Wei,<sup>b</sup> Xinyong Yu,<sup>b</sup> Lei Chen,<sup>a</sup> Xin Zhao,<sup>b</sup> Guoxing Tian<sup>b</sup> and Ling Chen<sup>id</sup><sup>\*bc</sup>

$\text{NiCo}_2\text{O}_4$ @reduced graphene oxide (rGO)/nickel foam (NF) composites were prepared via a hydrothermal method followed by annealing assisted by hexadecyl trimethyl ammonium bromide (CTAB).  $\text{NiCo}_2\text{O}_4$ @rGO/NF nanoneedle arrays grew directly on Ni foam (NF) without using a binder. The effect of graphene oxide (GO) concentration on the electrochemical properties of the composite was studied. When the GO concentration was  $5 \text{ mg L}^{-1}$ , the as-prepared  $\text{NiCo}_2\text{O}_4$ @rGO/NF reaches the highest specific capacitance of  $1644 \text{ F g}^{-1}$  at a current density of  $1 \text{ A g}^{-1}$ . Even at  $15 \text{ A g}^{-1}$ , the specific capacitance is still  $1167 \text{ F g}^{-1}$  and the capacitance retention rate is 89% after 10 000 cycles at  $10 \text{ A g}^{-1}$ . Furthermore, a  $\text{NiCo}_2\text{O}_4$ @rGO/NF/graphene hydrogel (GH) asymmetric supercapacitor cell (ASC) device was assembled and exhibits a high specific capacitance of  $84.13 \text{ F g}^{-1}$  at  $1 \text{ A g}^{-1}$  and excellent cycle stability (113% capacitance retention) after 10 000 charge/discharge cycles at  $10 \text{ A g}^{-1}$ . This provides potential for application in the field of supercapacitors due to the outstanding specific capacitance, rate performance and cycle stability of  $\text{NiCo}_2\text{O}_4$ @rGO/NF.

Received 17th December 2021  
Accepted 19th January 2022

DOI: 10.1039/d1ra09139e

rsc.li/rsc-advances

## 1. Introduction

With the aggravation of global warming and the exhaustion of fossil energy, the development and application of new energy materials are extremely urgent. On the one hand, new energy industries such as solar energy, wind energy and tidal power have promising prospects, but these energy sources have certain limitations in terms of time or space. In order to completely replace the original thermal power generation, matching energy storage systems are needed to achieve the continuous and stable output of electric energy. On the other hand, new energy vehicles represented by electric vehicles will replace traditional fuel vehicles to become the mainstream of transportation in the future, which will be a revolution in the world automobile industry and the inevitable result of low-carbon economic development. The key to overcome fuel vehicles is to develop

efficient energy storage devices with high energy density and power density, long cycle life and good safety. In addition, with the continuous progress of technology and the acceleration of informatization, there is an increasingly urgent demand for high-performance energy storage components in the military, industry, communication and other fields.

As efficient, environmentally friendly and new-type energy storage elements, supercapacitors have many advantages of both traditional capacitors and batteries, such as large capacitance, high energy density and power density, wide operating temperature range, long cycle life,<sup>1,2</sup> etc. They have attracted great attention in the world and become one of the important advanced technologies in the energy field. Electrode materials are the main component of supercapacitors and the key index to determine their performance. The research on the preparation and performance of electrode materials has always been the focus of the field of supercapacitors. Double-layer capacitor electrode materials represented by carbon materials<sup>3,4</sup> and pseudocapacitance electrode materials represented by transition metal oxides/hydroxides<sup>5-7</sup> and conductive polymers<sup>8,9</sup> have their own advantages, and considerable progress has been made in related researches. Among numerous transition metal oxides,  $\text{NiCo}_2\text{O}_4$  is a kind of mixed metal oxide with low price and abundant resource.<sup>10,11</sup>  $\text{NiCo}_2\text{O}_4$  is spinel structure, which can be considered to be formed by replacing Co with Ni in  $\text{Co}_3\text{O}_4$ . There are  $\text{Co}^{3+}/\text{Co}^{4+}$ ,  $\text{Ni}^{2+}/\text{Ni}^{3+}$  and  $\text{Co}^{2+}/\text{Co}^{3+}$  redox

<sup>a</sup>Northeast Petroleum University Qinhuangdao, Qinhuangdao, Hebei 066004, China. E-mail: 2008little@163.com; Fax: +86 335 8065113; Tel: +86 335 8065113

<sup>b</sup>Hebei Key Laboratory of Applied Chemistry, College of Environmental and Chemical Engineering, Yanshan University, Qinhuangdao, Hebei 066004, China. E-mail: hhchen@ysu.edu.cn; Fax: +86 335 8061569; Tel: +86 335 8061569

<sup>c</sup>Hebei Key Laboratory of Heavy Metal Deep-Remediation in Water and Resource Reuse, College of Environmental and Chemical Engineering, Yanshan University, Qinhuangdao, Hebei 066004, China

† Electronic supplementary information (ESI) available. See DOI: 10.1039/d1ra09139e



reaction pairs in the charge–discharge process. Therefore,  $\text{NiCo}_2\text{O}_4$  has higher electrochemical activity than pure nickel or cobalt oxides, and its electronic conductivity ( $10^{-1}$  to  $10^2 \text{ S cm}^{-1}$ ) is better than  $\text{Co}_3\text{O}_4$  and  $\text{NiO}$ .<sup>12,13</sup> Based on this,  $\text{NiCo}_2\text{O}_4$  has become the research hotspot of electrode materials for supercapacitors in recent years. However, its poor cycle stability and rate performance limit its application in practice. In order to improve the electrochemical properties of  $\text{NiCo}_2\text{O}_4$  materials, a lot of researches have been carried out.

The construction of special complex nanostructures is an effective strategy. Special nanostructures have significant effects on the properties of materials. Numerous  $\text{NiCo}_2\text{O}_4$  materials with various morphologies have been designed and synthesized, including nanosheets,<sup>14,15</sup> nanowires,<sup>16,17</sup> nanorods,<sup>11,18</sup> microspheres,<sup>19,20</sup> hexahedrons,<sup>21</sup> etc. These morphologies have their own advantages, but also have their limitations. One-dimensional nanostructures such as nanowires are beneficial to the assembly of nanodevices, but their own specific surface area is small and they cannot provide enough active sites in the reaction process. Two-dimensional nanostructures such as nanosheets have a large specific surface area, which can provide more electron transport channels and make full use of the active materials. However, nanosheets tend to form layered stacks, and their stability will decline after several charge–discharge cycles. Compared with simple structures, complex stereoscopic cross structures, such as core–shell structure<sup>22</sup> and yolk–shell structure<sup>23</sup> have more advantages in preventing internal particle agglomeration, providing more active sites for electrochemical reactions and effectively shortening ion diffusion paths. At the same time, the space between shells can buffer the residual pressure caused by volume expansion/contraction during the repeated Faraday reaction.

Besides,  $\text{NiCo}_2\text{O}_4$  compounds with different materials can combine the advantages of various materials and produce synergistic effect, which is expected to obtain more outstanding electrochemical performance. Most of the researches were focused on loading transition metal oxides such as  $\text{MnO}_2$ ,<sup>24</sup>  $\text{Ni}(\text{OH})_2$  (ref. 13) on the surface of  $\text{NiCo}_2\text{O}_4$ , or

loading  $\text{NiCo}_2\text{O}_4$  on porous materials with large surface area and high conductivity, such as nickel foam (NF)<sup>25</sup> and carbon materials,<sup>26</sup> etc. Among them, graphene as an infinitely scalable two-dimensional crystal material, which has a large specific surface area ( $2630 \text{ m}^2 \text{ g}^{-1}$ ), good electronic conductivity and chemical stability,<sup>27</sup> has been widely used in the preparation of composite electrode materials for supercapacitors since it was successfully isolated from graphite by Geim group in 2004.<sup>28</sup> In addition, one-dimensional carbon nanotubes (CNTs) are also commonly used in the preparation of composite materials.<sup>29</sup>

By integrating the above two approaches, the special composite microstructure constructed by integrating several materials with different structures is considered to be a more effective method to obtain excellent electrode materials for supercapacitors due to its good synergistic effect. Zhang *et al.*<sup>30</sup> synthesized reduced graphene oxide (rGO)/ $\text{NiCo}_2\text{O}_4$  composites, in which the rGO was coated on the  $\text{NiCo}_2\text{O}_4$  nanowires with no aggregation. The unique heterostructured rGO/ $\text{NiCo}_2\text{O}_4$  nanostructures exhibit high specific capacitance, excellent cycling stability and good rate capability in the application for supercapacitors, resulting from the interconnected porous frameworks and the strong interface polarization. Yang *et al.*<sup>31</sup> reported mesopores  $\text{NiCo}_2\text{O}_4$  nano-needles directly grown on nickel foam for high-performance supercapacitors by one-step hydrothermal method. The unique structure of mesopores increased the contact efficiency between the active materials and the electrolyte, which made the electrolyte easily penetrate the electrode and achieved a high capacitance response to have effective storage application. Wei *et al.*<sup>32</sup> developed a green pre-adjusted pH value aq. phase coprecipitation strategy assisted by citric acid, followed proper annealing at different temperature for the first time to synthesize novel honeycombed-like composites  $\text{NiCo}_2\text{O}_4/\text{rGO}$ .  $\text{NiCo}_2\text{O}_4/\text{rGO}$ -250 (at  $250^\circ\text{C}$ ) shows considerable specific capacitance, high rate performance and good cycling stability for supercapacitor, which could be attributed to the highly-ordered 3D honeycombed-like nano-sheet array leading to high specific surface area and numerous open macroporous network giving sufficient electroactive sites.

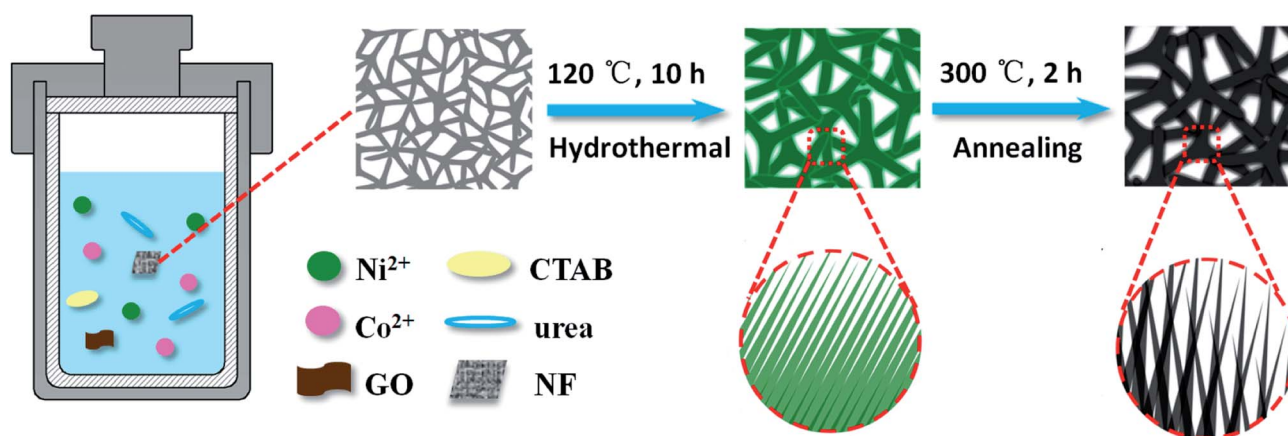


Fig. 1 Schematic synthesis procedure of  $\text{NiCo}_2\text{O}_4/\text{rGO}/\text{NF}$ .



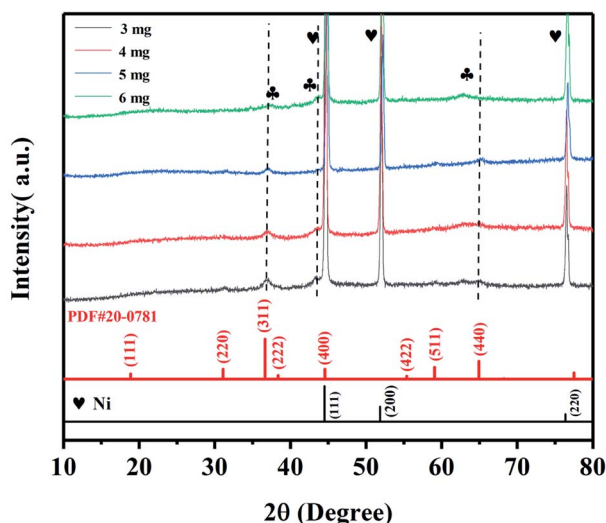


Fig. 2 XRD patterns of  $\text{NiCo}_2\text{O}_4@\text{rGO}/\text{NF}$  with different concentration of GO.

In brief, extensive researches revolved around the synthesis technology, morphology control, structural design and electrochemical performance improvement of  $\text{NiCo}_2\text{O}_4$  composites.

In this work, a simple strategy was used to prepare  $\text{NiCo}_2\text{O}_4@\text{rGO}/\text{NF}$  composites assisted by hexadecyl trimethyl ammonium bromide (CTAB) *via* hydrothermal method followed annealing. The prepared  $\text{NiCo}_2\text{O}_4@\text{rGO}/\text{NF}$  was applied to supercapacitors and the electrochemical performance was evaluated. In the process, the effect of graphene oxide (GO) concentration on the electrochemical properties of the composite was also investigated. It is believable that the synthetic strategy, the morphological control and the application of  $\text{NiCo}_2\text{O}_4@\text{rGO}/\text{NF}$  electrode materials with enhanced performance in the field of supercapacitor could provide reference for researchers.

## 2. Experimental

### 2.1. Preparation of $\text{NiCo}_2\text{O}_4@\text{rGO}/\text{NF}$ and $\text{NiCo}_2\text{O}_4/\text{NF}$

1 mmol of  $\text{Ni}(\text{NO}_3)_2 \cdot 6\text{H}_2\text{O}$ , 2 mmol of  $\text{Co}(\text{NO}_3)_2 \cdot 6\text{H}_2\text{O}$  and 4.5 mmol of urea were added into 20 mL of deionized water and stirred. Then 0.5 mmol of CTAB was added into the above solution with continuous stirring, and dispersed under ultrasonication for 30 min. GO was prepared by the modified Hummers' method.<sup>33</sup> A certain mass of GO was weighed and added into 10 mL of deionized water to form uniform dispersion under ultrasonication with a range of concentrations (3, 4,

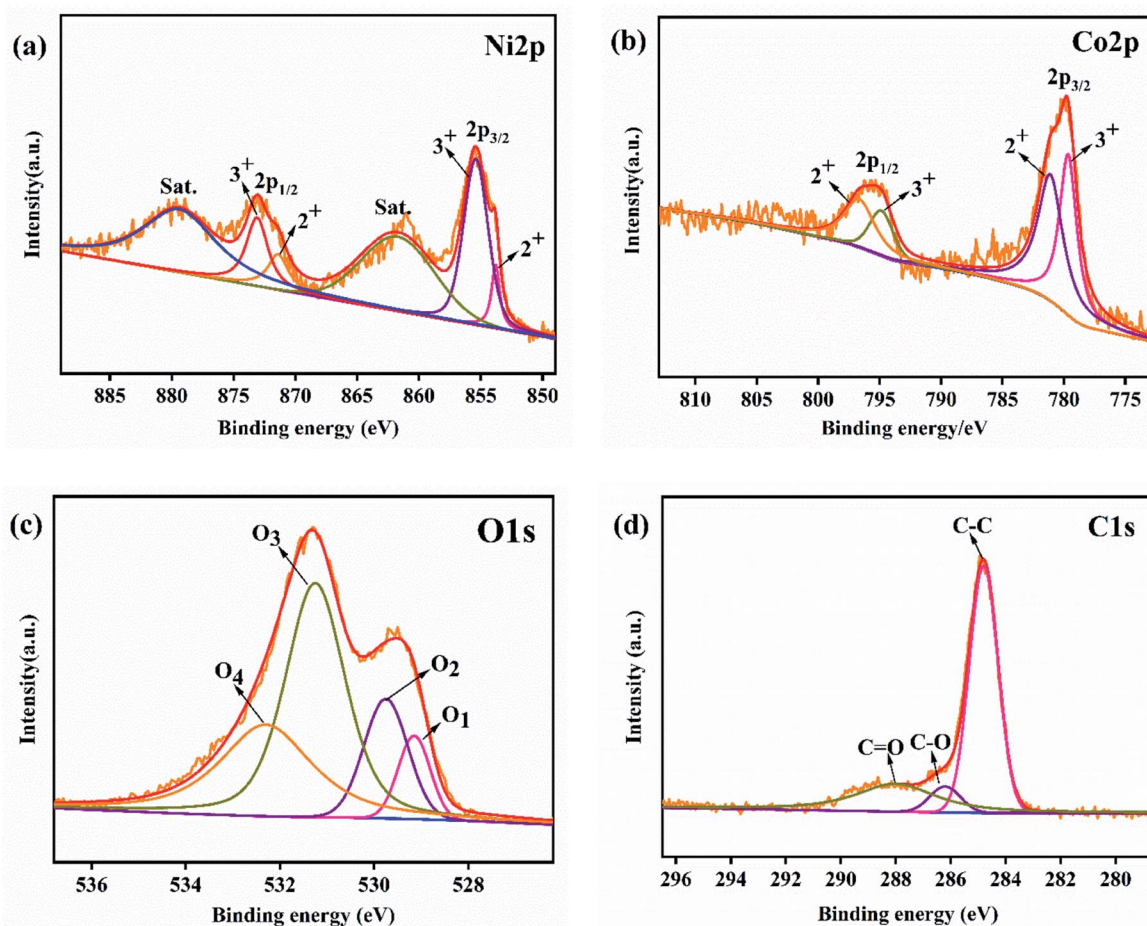


Fig. 3 XPS spectra of (a) Ni 2p, (b) Co 2p, (c) O 1s and (d) C 1s of the  $\text{NiCo}_2\text{O}_4@\text{rGO}/\text{NF}$  (GO 5  $\text{mg L}^{-1}$ ).





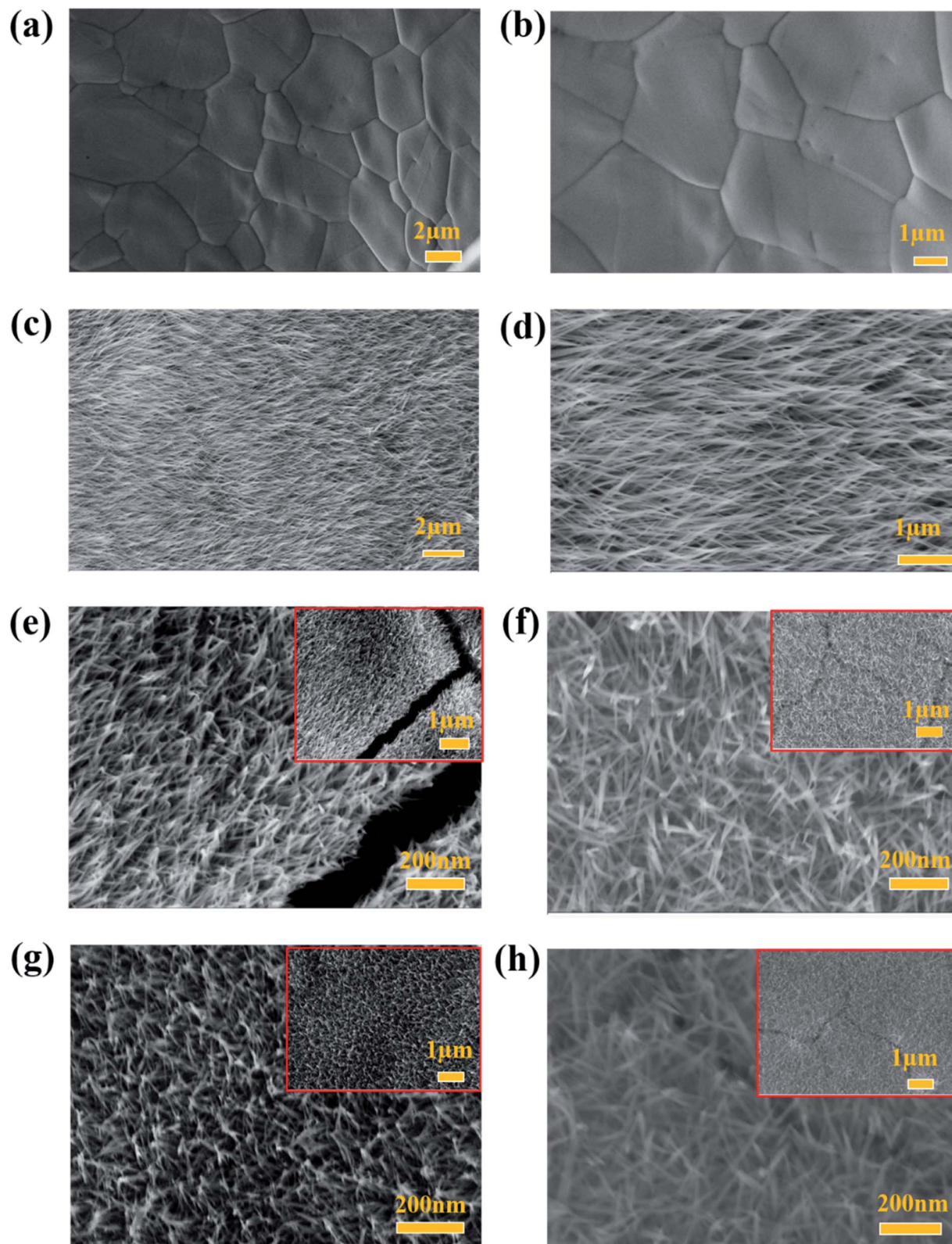


Fig. 4 SEM images of (a and b) bare Ni foam (c and d)  $\text{NiCo}_2\text{O}_4/\text{NF}$ , (e)  $\text{NiCo}_2\text{O}_4@\text{rGO}/\text{NF}$  ( $\text{GO } 3 \text{ mg L}^{-1}$ ), (f)  $\text{NiCo}_2\text{O}_4@\text{rGO}/\text{NF}$  ( $\text{GO } 4 \text{ mg L}^{-1}$ ), (g)  $\text{NiCo}_2\text{O}_4@\text{rGO}/\text{NF}$  ( $\text{GO } 5 \text{ mg L}^{-1}$ ) and (h)  $\text{NiCo}_2\text{O}_4@\text{rGO}/\text{NF}$  ( $\text{GO } 6 \text{ mg L}^{-1}$ ).



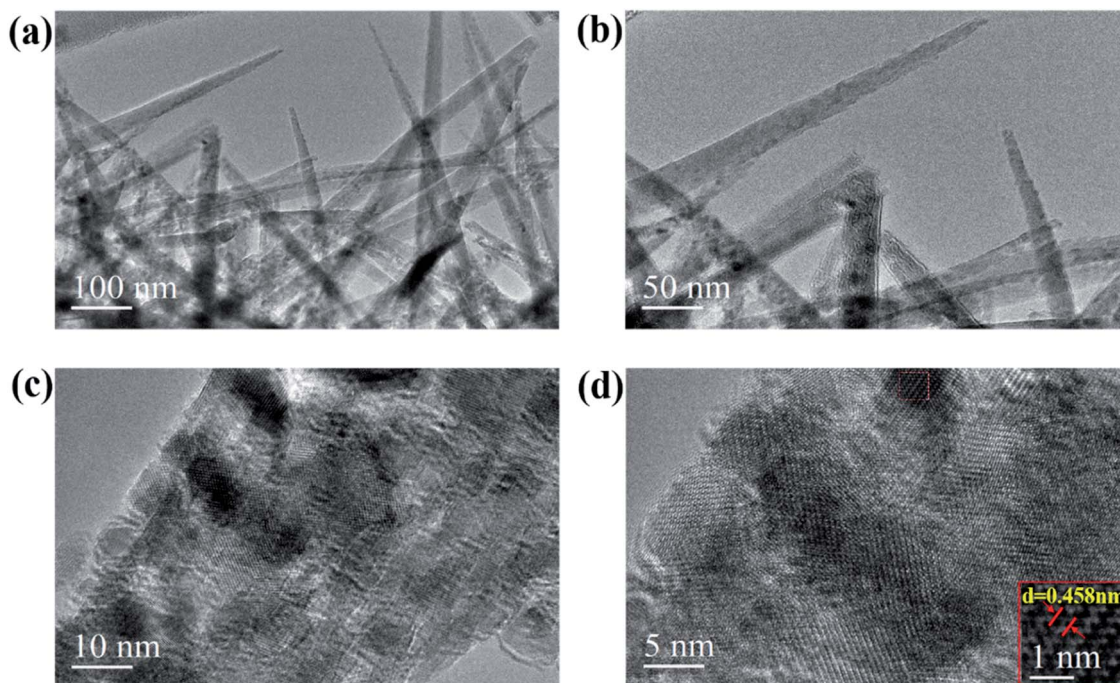


Fig. 5 (a, b) TEM and (c, d) HRTEM images of  $\text{NiCo}_2\text{O}_4@\text{rGO}/\text{NF}$  ( $\text{GO } 5 \text{ mg L}^{-1}$ ).

5 and 6  $\text{mg mL}^{-1}$ ) for later use. All the chemical reagents are of analytical grade.

The above two solutions were mixed and stirred for 40 min, then transferred into a Teflon lined stainless steel autoclave, in which a piece of nickel foam (NF) ( $1 \text{ cm} \times 1 \text{ cm}$ ) was immersed, then reacted at  $120^\circ\text{C}$  for 10 h. After cooling to room temperature, the nickel foam was rinsed with deionized water and ethanol. The product was dried at  $60^\circ\text{C}$  for 12 h. Finally,  $\text{NiCo}_2\text{O}_4@\text{rGO}/\text{NF}$  composites were obtained after annealing at  $300^\circ\text{C}$  for 2 h. Simultaneously,  $\text{NiCo}_2\text{O}_4/\text{NF}$  was synthesized by

the same way, but in absence of rGO for comparison. The schematic synthesis procedure of the  $\text{NiCo}_2\text{O}_4@\text{rGO}/\text{NF}$  composites is illustrated in Fig. 1. In brief, firstly,  $\text{NiCo}_2(\text{OH})_6$  was formed in the hydrothermal reaction,<sup>34</sup> and CTAB played a role of controlling the morphology of the products during the reaction.<sup>35</sup> Then,  $\text{NiCo}_2\text{O}_4$  was acquired after further heat treatment.

## 2.2. Characterization

The phase structures of the as-prepared materials were performed using the powder X-ray diffraction (XRD, D-max-2500/

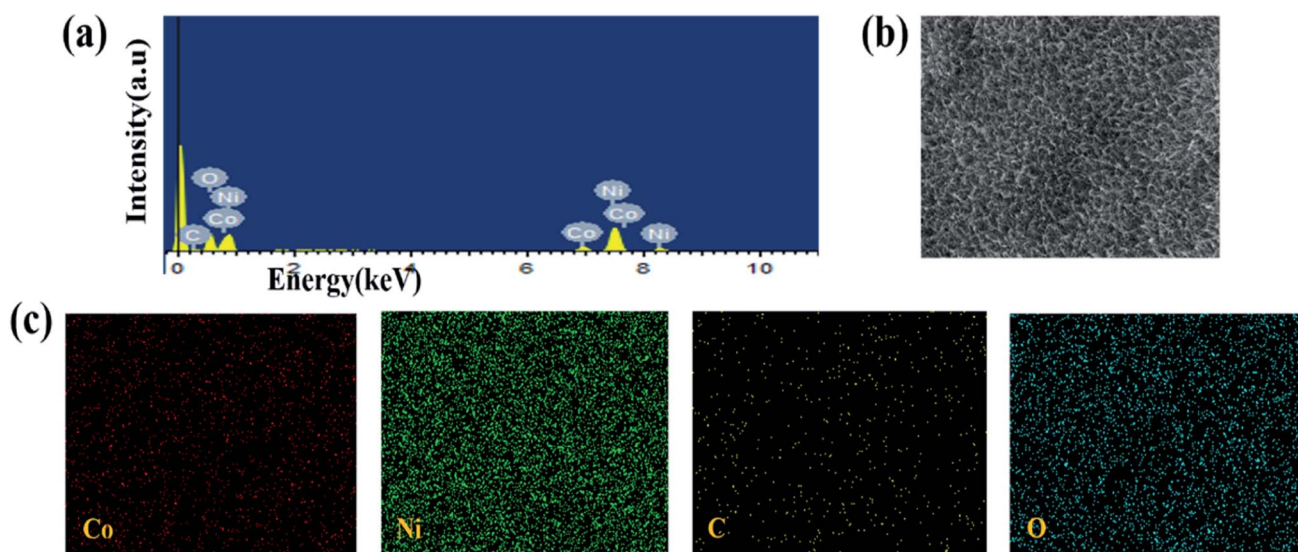


Fig. 6 (a) SEM energy dispersive spectroscopy, (b) SEM and (c) SEM element mapping of  $\text{NiCo}_2\text{O}_4@\text{rGO}/\text{NF}$  ( $\text{GO } 5 \text{ mg L}^{-1}$ ).



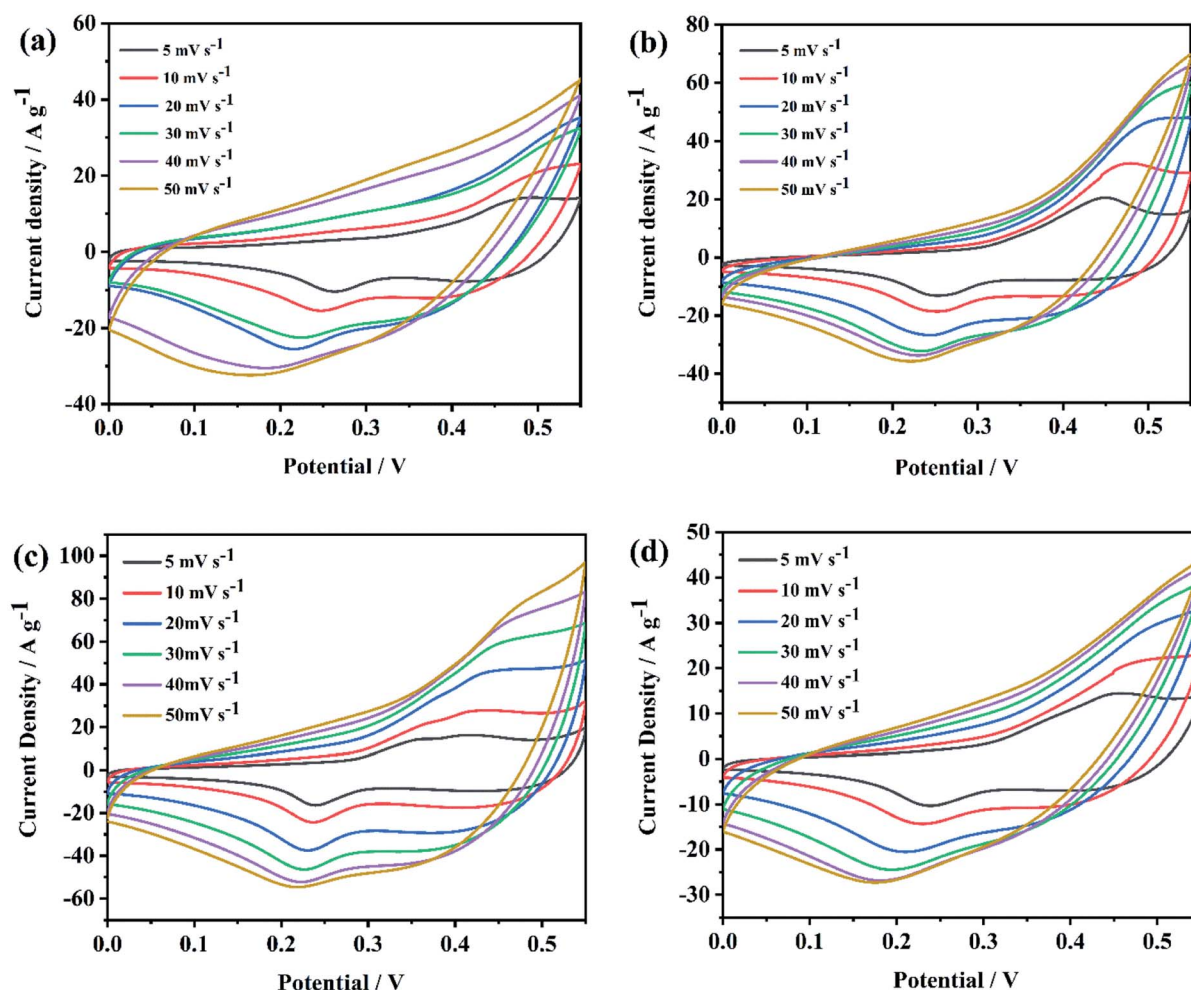


Fig. 7 CV curves of NiCo<sub>2</sub>O<sub>4</sub>@rGO/NF with different concentration of GO at various scan rates: (a) NiCo<sub>2</sub>O<sub>4</sub>@rGO/NF (GO 3 mg L<sup>-1</sup>), (b) NiCo<sub>2</sub>O<sub>4</sub>@rGO/NF (GO 4 mg L<sup>-1</sup>), (c) NiCo<sub>2</sub>O<sub>4</sub>@rGO/NF (GO 5 mg L<sup>-1</sup>) and (d) NiCo<sub>2</sub>O<sub>4</sub>@rGO/NF (GO 6 mg L<sup>-1</sup>).

PC, Rigaku) with Cu K $\alpha$  radiation ( $\lambda = 0.15406$  nm) over a range  $2\theta = 10^\circ$ – $80^\circ$ . The morphologies were characterized by scanning electron microscopy (SEM, KYKY-2800B) and transmission electron microscopy (TEM, Hitachi HT-7700). The elemental analysis was detected by X-ray photoelectron spectroscopy (XPS, Thermal ESCALAB 250).

### 2.3. Electrochemical measurements

The nickel foam loaded with active material was pressed under a pressure of 10 MPa, and then soaked in 6 M KOH solution for 24 h. The electrochemical performance was tested in a three-electrode system with 6 M KOH aqueous as the electrolyte. The as-prepared active material was used as the working electrode, platinum plate (1 cm  $\times$  1 cm) electrode as the counter electrode and Hg/HgO electrode as the reference electrode. Galvanostatic charge–discharge (GCD) tests were performed *via* a charge–discharge instrument (Neware CT-3008, Shenzhen, China) with a potential window of 0–0.45 V. Cyclic voltammetry (CV) and electrochemical impedance spectroscopy (EIS) were carried out on a CHI660E electrochemical workstation

(Chenhua, Shanghai, China). The potential range of CV tests was from 0 V to 0.55 V, and the frequency range of EIS was from  $10^{-2}$  Hz to  $10^5$  Hz with the amplitude of 5 mV.

## 3. Results and discussion

### 3.1. Structure and morphology

The XRD patterns of NiCo<sub>2</sub>O<sub>4</sub>@rGO/NF composites with different concentration of GO (3, 4, 5 and 6 mg mL<sup>-1</sup>) are shown in Fig. 2. The diffraction peaks of the composites obtained at different concentrations of GO are basically the same. It indicates that the amount of GO in the preparation of the composites had no effect on the phase of NiCo<sub>2</sub>O<sub>4</sub>. Three strong and sharp diffraction peaks are corresponded to nickel deriving from the foam nickel substrate. The diffraction peaks of  $2\theta$  at  $36.7^\circ$ ,  $44.6^\circ$ ,  $59.1^\circ$  and  $64.9^\circ$  can be indexed to NiCo<sub>2</sub>O<sub>4</sub> (JCPDS 20-0781), corresponding to (311), (400), (511) and (440) crystal planes, respectively. There is no obvious diffraction peak of rGO observed, which probably because the characteristic peak of rGO was covered by three strong peaks of nickel.<sup>36</sup> The chemical states of NiCo<sub>2</sub>O<sub>4</sub>@rGO/NF (GO 5 mg L<sup>-1</sup>) are characterized by



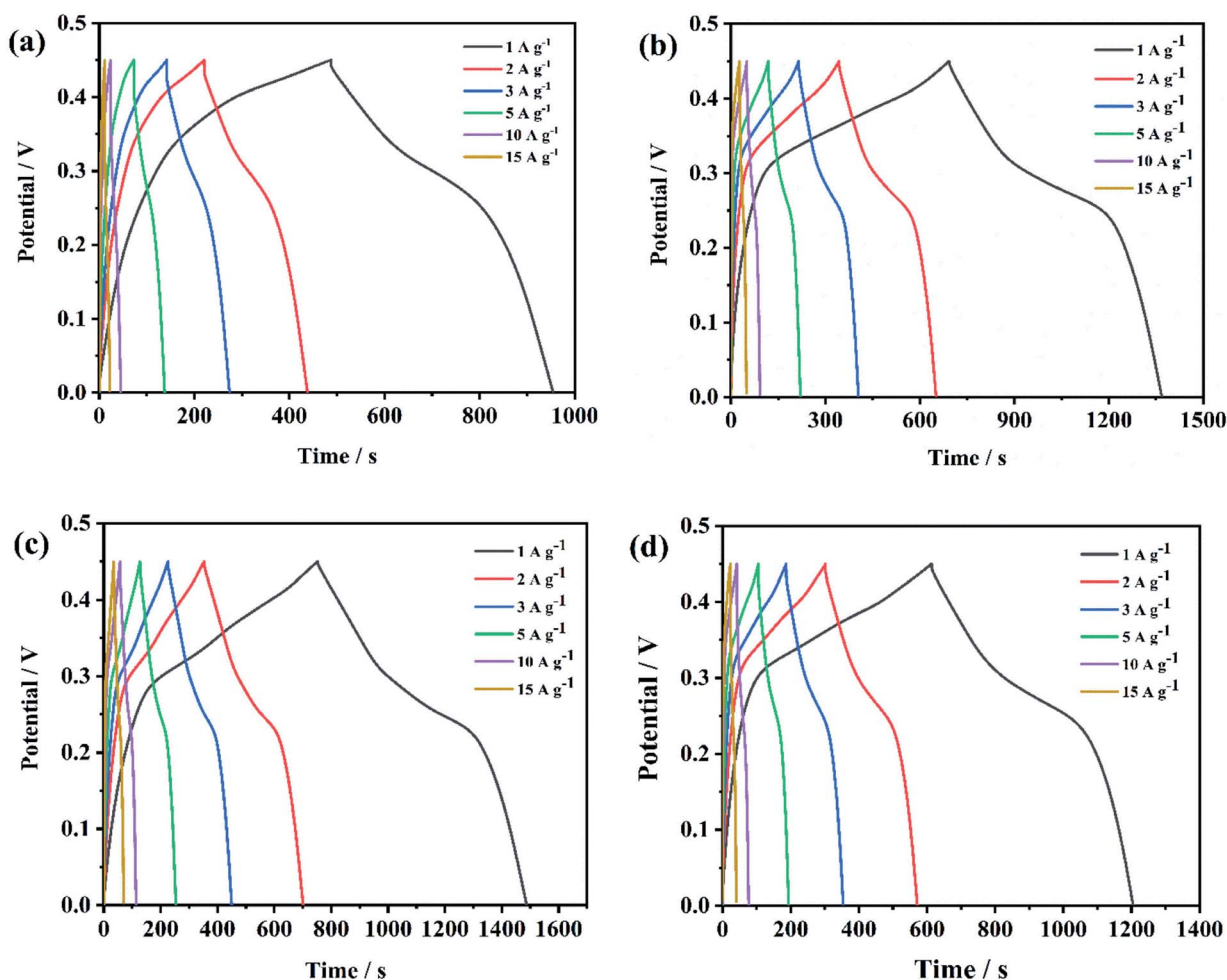


Fig. 8 GCD curves of NiCo<sub>2</sub>O<sub>4</sub>@rGO/NF with different concentration of GO at various current densities: (a) NiCo<sub>2</sub>O<sub>4</sub>@rGO/NF (GO 3 mg L<sup>-1</sup>), (b) NiCo<sub>2</sub>O<sub>4</sub>@rGO/NF (GO 4 mg L<sup>-1</sup>), (c) NiCo<sub>2</sub>O<sub>4</sub>@rGO/NF (GO 5 mg L<sup>-1</sup>) and (d) NiCo<sub>2</sub>O<sub>4</sub>@rGO/NF (GO 6 mg L<sup>-1</sup>).

XPS, as shown in Fig. 3, the region spectra of Ni 2p, Co 2p, O 1s and C 1s show characteristic peaks. The Ni 2p shows the peaks of Ni 2p<sub>3/2</sub> and Ni 2p<sub>1/2</sub> (Fig. 3(a)), both consisting of doublet peaks at 853.8, 855.4, 871.4 and 873.1 eV, corresponding to Ni<sup>2+</sup> 2p<sub>3/2</sub>, Ni<sup>3+</sup> 2p<sub>3/2</sub>, Ni<sup>2+</sup> 2p<sub>1/2</sub>, and Ni<sup>3+</sup> 2p<sub>1/2</sub>, respectively,<sup>37</sup> which could imply the presence of both Ni<sup>2+</sup> and Ni<sup>3+</sup>. Two fitting peaks corresponding to Co 2p<sub>3/2</sub> and Co 2p<sub>1/2</sub> were observed in the Co 2p spectrum (Fig. 3(b)), which are characteristic of Co<sup>2+</sup> and Co<sup>3+</sup>. The doublet peaks at 779.65 and 781.1 eV correspond to Co<sup>3+</sup> 2p<sub>3/2</sub> and Co<sup>3+</sup> 2p<sub>1/2</sub> as well as the other two at 794.85 and 796.65 eV correspond to Co<sup>2+</sup> 2p<sub>3/2</sub> and Co<sup>2+</sup> 2p<sub>1/2</sub>.<sup>38</sup> The spectrum of O 1s region (Fig. 3(c)) can be deconvoluted into four peaks at 529.15, 529.75, 531.25 and 532.3 eV, represented as O<sub>1</sub>, O<sub>2</sub>, O<sub>3</sub> and O<sub>4</sub>, which are assigned to metal-oxygen bonds in the lattice of NiCo<sub>2</sub>O<sub>4</sub>, the surface hydroxyl, defect sites and physical/chemical adsorbed water, respectively.<sup>39,40</sup> The C 1s spectrum (Fig. 3(d)) displays three types carbon bonds, including sp<sup>2</sup> C-C (284.8 eV), C-O (286.2 eV) and C=O (288.0 eV).<sup>41</sup> It also can be seen from the peak intensity that the amount of oxygen-containing functional groups is less than that of C-C groups, indicating the successful reduction of GO to rGO.<sup>40</sup>

The morphologies and nanostructures of bare Ni foam, NiCo<sub>2</sub>O<sub>4</sub>/NF and NiCo<sub>2</sub>O<sub>4</sub>@rGO/NF with different concentrations of GO (3, 4, 5 and 6 mg L<sup>-1</sup>) are characterized by SEM and the images are shown in Fig. 4. As shown in Fig. 4(a and b), the surface of bare Ni foam is smooth. After hydrothermal reaction, double hydroxides precursor of NiCo<sub>2</sub>O<sub>4</sub> was formed, which presents nanowire morphology (Fig. S1, ESI†). After heat treatment, when GO was in absence, the NF is completely covered by NiCo<sub>2</sub>O<sub>4</sub> nanoneedle arrays, which are neatly oriented (Fig. 4(c and d)). When GO was added, the product of NiCo<sub>2</sub>O<sub>4</sub>@rGO still maintains nanoneedle morphology. However, it's important to point out that the nanoneedles crossed in different directions, as shown in Fig. 4(e-h). The difference in morphology is mainly due to the role of rGO. NF provided growth sites for NiCo<sub>2</sub>O<sub>4</sub>, and then nanoneedles' growth was prolonged and strongly isotropic. In the presence of rGO, rGO adsorbed to NF and then coated and separated NiCo<sub>2</sub>O<sub>4</sub>, which changed its growth direction and led to the anisotropy. As the concentration of GO increased, rGO cladding layers in the composites would be thickened. Fig. 5(a and b) show different magnified TEM images of NiCo<sub>2</sub>O<sub>4</sub>@rGO composites (GO 5 mg L<sup>-1</sup>), from which it



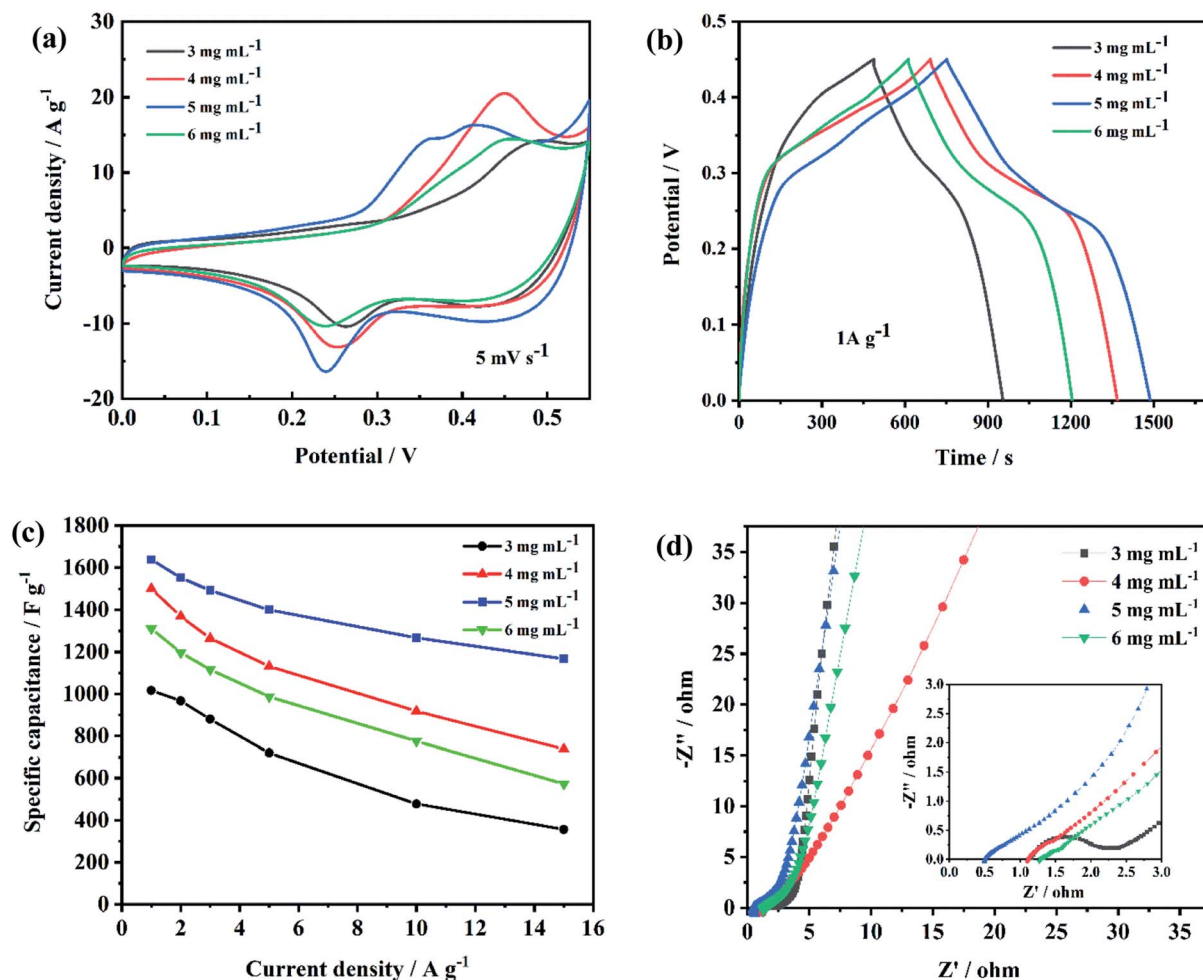
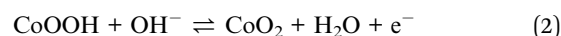


Fig. 9 Comparison of electrochemical performance of NiCo<sub>2</sub>O<sub>4</sub>@rGO/NF with different concentration of GO: (a) CV curves (5 mV s<sup>-1</sup>), (b) GCD curves (1 A g<sup>-1</sup>), (c) specific capacitances at various current densities and (d) Nyquist plots of EIS.

could be clearly observed that NiCo<sub>2</sub>O<sub>4</sub> nanoneedles are interlaced. From HRTEM images (Fig. 5(c and d)), it can be seen that a lattice spacing of 0.458 nm corresponding to the (111) crystal plane of NiCo<sub>2</sub>O<sub>4</sub>. The SEM energy dispersive spectroscopy (EDS) in Fig. 6(a) verifies the existence of C, O, Ni and Co elements. As can be seen from the SEM (Fig. 6(b)) mapping images in Fig. 6(c), Co, Ni, C, and O distribute homogeneously over the NiCo<sub>2</sub>O<sub>4</sub>@rGO architecture. It also proves the existence and distribution of rGO in the composites.

### 3.2. Electrochemical performance

Fig. 7 shows CV curves of NiCo<sub>2</sub>O<sub>4</sub>@rGO/NF with different concentration of GO (3, 4, 5, 6 mg L<sup>-1</sup>), which were carried out at the potential window from 0 to 0.55 V with the scan rate of 5, 10, 20, 30, 40 and 50 mV s<sup>-1</sup>. There is a pair of redox peaks can be observed on all CV curves (Fig. 7(a-d)), which resulted from redox reactions of Co<sup>3+</sup>/Co<sup>4+</sup>, Ni<sup>2+</sup>/Ni<sup>3+</sup> and Co<sup>2+</sup>/Co<sup>3+</sup>, demonstrating the pseudocapacitive characteristic of NiCo<sub>2</sub>O<sub>4</sub>@rGO/NF composite.<sup>42</sup> The reaction equations are as follows:<sup>43</sup>



When the scan rate increased from 5 to 50 mV s<sup>-1</sup>, the shape of CV curves had little change, suggesting good electrochemical reversibility as supercapacitor electrodes. GCD curves of NiCo<sub>2</sub>O<sub>4</sub>@rGO/NF with different concentration of GO (3, 4, 5, 6 mg L<sup>-1</sup>) at the various current density of 1, 2, 3, 5, 10 and 15 A g<sup>-1</sup> are displayed in Fig. 8. From (Fig. 8(a)-(d)) can we see, the charge-discharge curves are all nonlinear with evident voltage plateau, indicating typical pseudocapacitive behavior, which is consistent with the CV results. For a comparison, the electrochemical performance of NiCo<sub>2</sub>O<sub>4</sub>@rGO/NF composites with different concentration of GO were contrasted and depicted in Fig. 9. When the concentration of GO was 5 mg L<sup>-1</sup>, the closed area of CV curve is the largest (Fig. 9(a)) and the GCD curve has the longest discharge time (Fig. 9(b)). The specific capacitance calculated by the GCD curve is 1044, 1504, 1644 and 1322 F g<sup>-1</sup>, corresponding to GO concentration of 3, 4, 5 and 6 mg L<sup>-1</sup>, respectively. At all the current densities, NiCo<sub>2</sub>O<sub>4</sub>@rGO/NF (GO 5 mg L<sup>-1</sup>) has the largest specific capacitance compared with the samples of the other three concentrations.





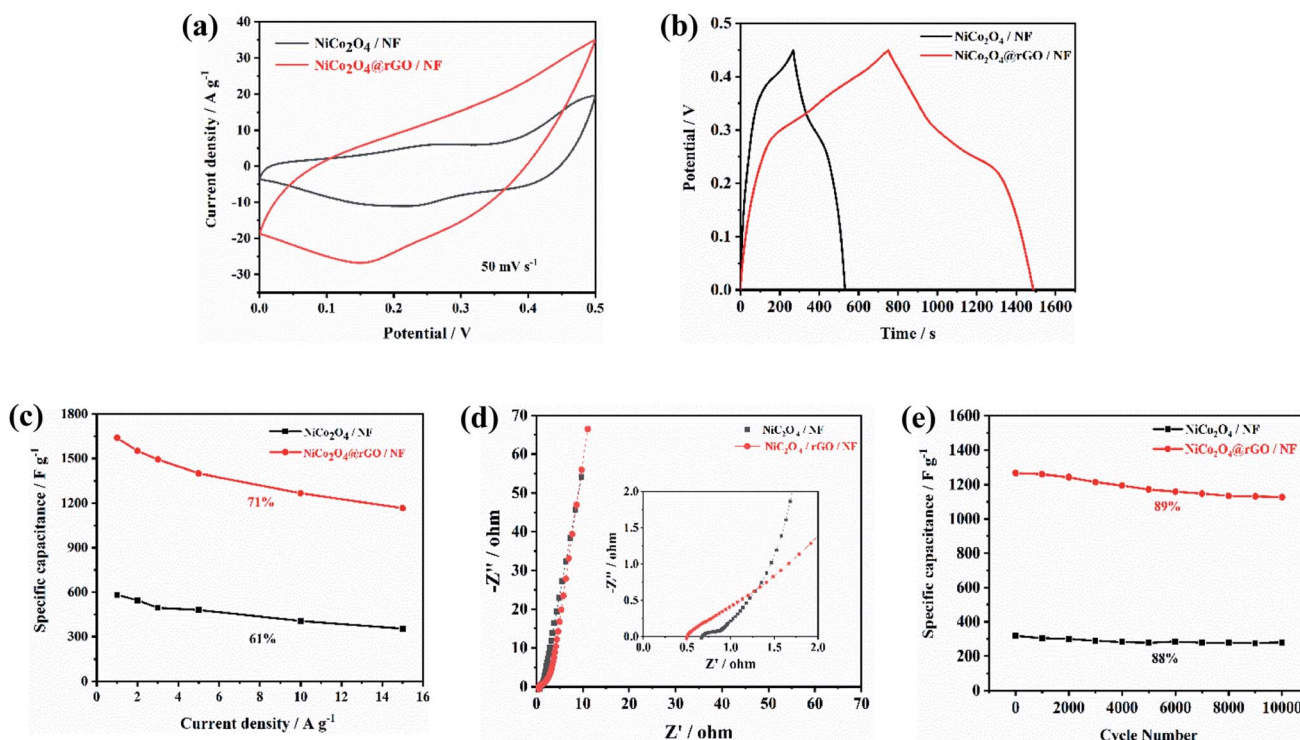


Fig. 10 Comparison of electrochemical performance of NiCo<sub>2</sub>O<sub>4</sub>@rGO/NF with NiCo<sub>2</sub>O<sub>4</sub>/NF: (a) CV curves (50 mV s<sup>-1</sup>), (b) GCD curves (1 A g<sup>-1</sup>), (c) specific capacitances at different current densities, (d) Nyquist plots of EIS and (e) cycling stability (10 A g<sup>-1</sup>).

Moreover, its specific capacitance varies most gently with the current density, suggesting good rate performance (Fig. 9(c)). It is probably because that as the concentration of GO increased, the proportion of rGO in NiCo<sub>2</sub>O<sub>4</sub>@rGO/NF composite increased, and rGO plays a role in connecting NiCo<sub>2</sub>O<sub>4</sub> nanoneedles to improve the electrical conductivity of the composite. However, due to the low specific capacitance of rGO itself, too much rGO will affect the overall specific capacitance of the composite. Nyquist plots of EIS for NiCo<sub>2</sub>O<sub>4</sub>@rGO/NF composites with various concentrations (3, 4, 5 and 6 mg L<sup>-1</sup>) are shown in Fig. 9(d). The line at low frequency region of NiCo<sub>2</sub>O<sub>4</sub>@rGO/NF (GO 5 mg L<sup>-1</sup>) is more vertical to the real axis (Z'), indicating more ideal capacitance behavior.<sup>44</sup>

Fig. 10 describes the comparison of electrochemical properties of NiCo<sub>2</sub>O<sub>4</sub>@rGO/NF and NiCo<sub>2</sub>O<sub>4</sub>/NF. As shown in Fig. 10(a), the CV curves of NiCo<sub>2</sub>O<sub>4</sub>@rGO/NF and NiCo<sub>2</sub>O<sub>4</sub>/NF at the scan rate of 50 mV s<sup>-1</sup>, NiCo<sub>2</sub>O<sub>4</sub>@rGO/NF has larger closed area than NiCo<sub>2</sub>O<sub>4</sub>/NF, demonstrating higher specific capacitance. It is confirmed by GCD tests, displayed in Fig. 10(b). At the current density of 1 A g<sup>-1</sup>, the specific capacitance of NiCo<sub>2</sub>O<sub>4</sub>/NF and NiCo<sub>2</sub>O<sub>4</sub>@rGO/NF is 582.2 and 1644 F g<sup>-1</sup>, respectively. Obviously, it is nearly twice higher the composite with rGO than that without rGO. Fig. 10(c) shows the specific capacitance of these two composites changing with the current density. The calculated specific capacitance of NiCo<sub>2</sub>O<sub>4</sub>@rGO/NF is 1644, 1551, 1493, 1400, 1267 and 1167 F g<sup>-1</sup> at the current density of 1, 2, 3, 5, 10 and 15 A g<sup>-1</sup>. Even at 15 A g<sup>-1</sup>, 71% of the specific capacitance (1 A g<sup>-1</sup>) has still been retained, while the specific capacitance retention of NiCo<sub>2</sub>O<sub>4</sub>/NF is 61%. It can be

seen that NiCo<sub>2</sub>O<sub>4</sub>@rGO/NF has better rate performance. Nyquist plots of EIS for NiCo<sub>2</sub>O<sub>4</sub>@rGO/NF and NiCo<sub>2</sub>O<sub>4</sub>/NF are shown in Fig. 10(d). The intercept at the real axis represents the equivalent series resistance ( $R_s$ ), containing the electrolyte resistance, the intrinsic resistance and the contact resistance. The diameter of the semicircle at the high frequency is associated with the charge-transfer resistance ( $R_{ct}$ ). For NiCo<sub>2</sub>O<sub>4</sub>@rGO/NF and NiCo<sub>2</sub>O<sub>4</sub>/NF electrodes, the  $R_s$  values are 0.679 and 0.501  $\Omega$ , respectively, indicating that a lower solution resistance of NiCo<sub>2</sub>O<sub>4</sub>@rGO/NF than that of NiCo<sub>2</sub>O<sub>4</sub>/NF. Likewise, NiCo<sub>2</sub>O<sub>4</sub>@rGO/NF has a smaller semicircle, which could provide a fast pathway for ion transfer and electron transport. The cycle stability of the two electrodes after 10 000 cycles was tested at a current density of 10 A g<sup>-1</sup>. As shown in Fig. 10(e), it is obvious that the specific capacitance of NiCo<sub>2</sub>O<sub>4</sub>@rGO/NF composite is much higher than that of NiCo<sub>2</sub>O<sub>4</sub>/NF. Additionally, NiCo<sub>2</sub>O<sub>4</sub>@rGO/NF can still maintain 89% of the initial specific capacitance after 10 000 charge-discharge cycles, exhibiting more excellent cycle stability than NiCo<sub>2</sub>O<sub>4</sub>/NF. The electrochemical properties of NiCo<sub>2</sub>O<sub>4</sub> and its composite materials reported in some literatures are listed in Table 1. It can be seen from the literature comparison, the NiCo<sub>2</sub>O<sub>4</sub>@rGO/NF composite prepared in this work is comparable. In brief, the superiority of electrochemical performance of NiCo<sub>2</sub>O<sub>4</sub>@rGO/NF composite is mainly analyzed for the following reasons: (i) the anisotropic nanoneedles formed a cross network, which could provide an effective channel for ion/electron diffusion. (ii) NiCo<sub>2</sub>O<sub>4</sub> grows directly on NF matrix, and rGO plays a bridge among the NiCo<sub>2</sub>O<sub>4</sub> nanoneedles, together with no binder is used, which have effectively improve the conductivity of



**Table 1** Comparison of electrochemical performance of NiCo<sub>2</sub>O<sub>4</sub>@rGO/NF in this work with previous literatures

Materials	Specific capacitance	Cycle stability	Rate performance	References
rGO/NiCo <sub>2</sub> O <sub>4</sub>	1248 F g <sup>-1</sup> (2 mA cm <sup>-2</sup> )	90% (5 mA cm <sup>-2</sup> ) 2000 cycles	59% (2–10 mA cm <sup>-2</sup> )	30
NiCo <sub>2</sub> O <sub>4</sub> nano-needles/NF	1410 F g <sup>-1</sup> (1 A g <sup>-1</sup> )	94.7% (20 A g <sup>-1</sup> ) 3000 cycles	73.8% (1–20 A g <sup>-1</sup> )	31
NiCo <sub>2</sub> O <sub>4</sub> /rGO	1380 F g <sup>-1</sup> (1 A g <sup>-1</sup> )	90% (5 A g <sup>-1</sup> ) 1000 cycles	70% (1–10 A g <sup>-1</sup> )	32
rGO@NiCo <sub>2</sub> O <sub>4</sub> NFs	1040 F g <sup>-1</sup> (1 A g <sup>-1</sup> )	88% (30 A g <sup>-1</sup> ) 5000 cycles	88.8% (1–10 A g <sup>-1</sup> )	45
NiCo <sub>2</sub> O <sub>4</sub> @NF	646.6 F g <sup>-1</sup> (1 A g <sup>-1</sup> )	96.5% (7 A g <sup>-1</sup> ) 3000 cycles (ASC)	32% (1–9 A g <sup>-1</sup> )	46
NiCo <sub>2</sub> O <sub>4</sub> @rGO/NF	1644 F g <sup>-1</sup> (1 A g <sup>-1</sup> )	89% (10 A g <sup>-1</sup> ) 10 000 cycles	71% (1–15 A g <sup>-1</sup> )	This work

the composite, due to the excellent electrical conductivity of NF and rGO. Furthermore, it also plays a positive role in the full use of active materials. (iii) The outstanding mechanical property inhibits the deformation caused by swelling/shrinking of the electrode material during the repeated charge–discharge process.

In addition, the asymmetric supercapacitor cell (ASC) was fabricated from two-electrode devices by using the prepared NiCo<sub>2</sub>O<sub>4</sub>@rGO/NF as the positive electrode and graphene hydrogel (GH) as the negative electrode in 6 M KOH electrolyte, illustrated in Fig. 11(a). As shown in Fig. 11(b), the CV curve of NiCo<sub>2</sub>O<sub>4</sub>@rGO/NF positive electrode exhibits a potential range of 0 V to 0.55 V, whereas that of GH negative electrode shows

a range of −1.0 V to 0 V. Therefore, CV measurements of NiCo<sub>2</sub>O<sub>4</sub>@rGO/NF//GH ASC were carried out at an operating potential window of 0 V to 1.55 V with the scan rate of 5, 10, 20, 50 and 100 mV s<sup>-1</sup> (Fig. 11(c)), which indicate that the CV curves at all the scan rates retain both the pseudocapacitive characteristic and electrochemical double layer capacitance (EDLC). Besides, the redox peak has a slight movement with the increase of the scan rate, perhaps owing to the electrode polarization.<sup>47</sup> Fig. 11(d) depicts GCD curves of NiCo<sub>2</sub>O<sub>4</sub>@rGO/NF//GH ASC at various current densities on the potential window of 0 V to 1.55 V. With the increase of the current density, the curves could maintain an approximate symmetrical triangle, showing good

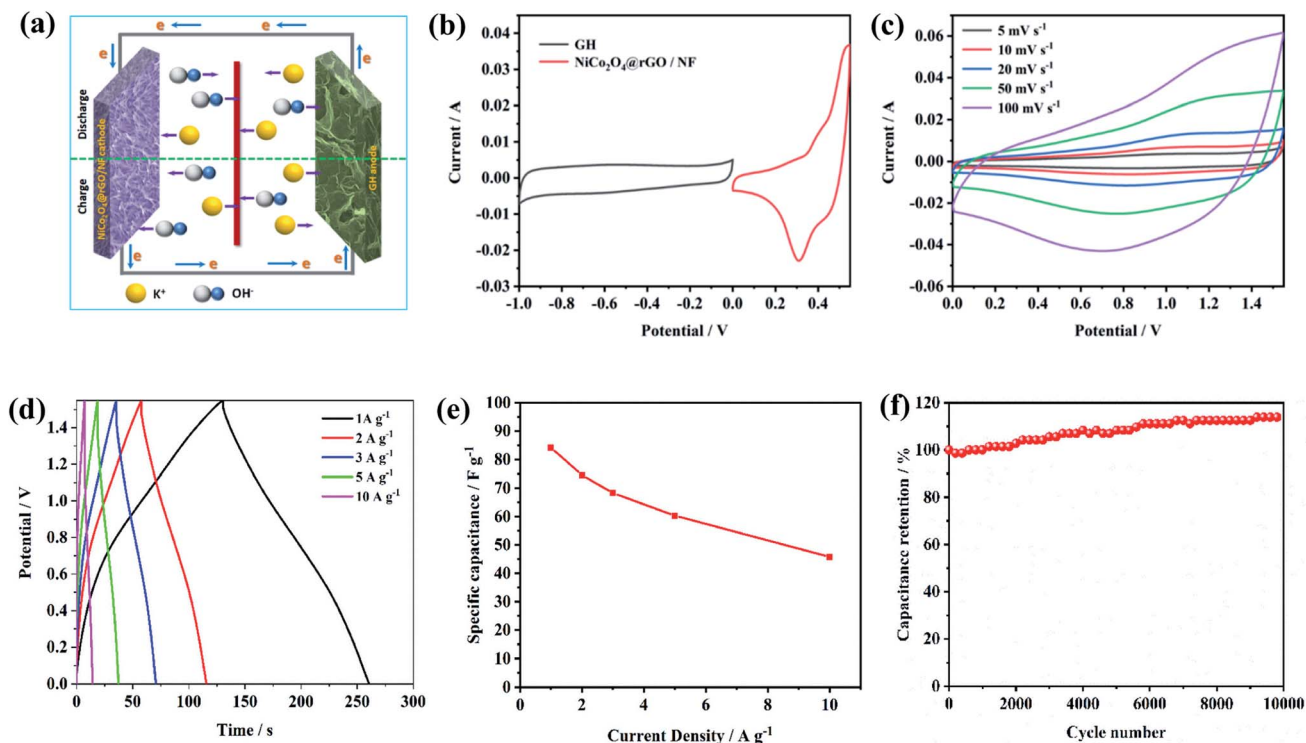


**Fig. 11** (a) Schematic of the fabricated NiCo<sub>2</sub>O<sub>4</sub>@rGO/NF//GH asymmetric supercapacitor device, (b) CV curves of GH anode and NiCo<sub>2</sub>O<sub>4</sub>@rGO/NF cathode electrodes (5 mV s<sup>-1</sup>), (c) CV curves of NiCo<sub>2</sub>O<sub>4</sub>@rGO/NF//GH at various scan rates, (d) GCD curves of NiCo<sub>2</sub>O<sub>4</sub>@rGO/NF//GH at various current densities, (e) specific capacitances of NiCo<sub>2</sub>O<sub>4</sub>@rGO/NF//GH at various current densities and (f) cycling performance of NiCo<sub>2</sub>O<sub>4</sub>@rGO/NF//GH device (10 A g<sup>-1</sup>).



reversibility. The calculated specific capacitance of the ASC device is 84.13, 74.58, 68.32, 60.32 and 45.81 F g<sup>-1</sup> at the current density of 1, 2, 3, 5 and 10 A g<sup>-1</sup>, respectively. The rate performance of NiCo<sub>2</sub>O<sub>4</sub>@rGO/NF//GH ASC is displayed in Fig. 11(e). When the current density increased to 10 A g<sup>-1</sup>, it could still maintain 54.5% of the specific capacitance at 1 A g<sup>-1</sup>. Fig. 11(f) describes the cycle performance of NiCo<sub>2</sub>O<sub>4</sub>@rGO/NF//GH ASC at a current density of 10 A g<sup>-1</sup>. After 10 000 cycles, the specific capacitance increased to 51.76 F g<sup>-1</sup>, which is 113% of the initial value (45.81 F g<sup>-1</sup>), which is probably because of the electrolyte has fully penetrated into the material, making the active material be more fully utilized with the continuous charge–discharge cycles, demonstrating excellent cycle stability of NiCo<sub>2</sub>O<sub>4</sub>@rGO/NF//GH ASC device.

## 4. Conclusion

In conclusion, NiCo<sub>2</sub>O<sub>4</sub>@rGO/NF composite electrode materials with enhanced supercapacitive performance were synthesized by a simple hydrothermal method assisted by CTAB combined with subsequent heat treatment. The aeolotropic NiCo<sub>2</sub>O<sub>4</sub>@rGO nanoneedles grew directly on Ni foam with rGO connecting to each other and without any binder, which has greatly improved the conductivity of electrode materials. Moreover, the crossed network also provides a pathway for ion diffusion. For supercapacitor application, the highest specific capacitance of NiCo<sub>2</sub>O<sub>4</sub>@rGO/NF could reach 1644 F g<sup>-1</sup> at a current density of 1 A g<sup>-1</sup>, and even at 15 A g<sup>-1</sup>, the value still maintain 1167 F g<sup>-1</sup>, additionally, there is 89% capacitance retention after 10 000 cycles at 10 A g<sup>-1</sup>. Furthermore, NiCo<sub>2</sub>O<sub>4</sub>@rGO/NF//GH ASC device was assembled and exhibits a high specific capacitance of 84.13 F g<sup>-1</sup> (1 A g<sup>-1</sup>) and excellent cycle stability (113% capacitance retention after 10 000 charge/discharge cycles at 10 A g<sup>-1</sup>). Higher specific capacitance, better rate performance and cycle stability highlight the advantages of NiCo<sub>2</sub>O<sub>4</sub>@rGO/NF composites as electrode materials for supercapacitors, associating with the regulated morphology, suitable GO concentration synergy of components. As one of the most promising materials, it is believed that NiCo<sub>2</sub>O<sub>4</sub>@rGO/NF will have a broader application prospect in the future.

## Conflicts of interest

There are no conflicts to declare.

## Acknowledgements

We are grateful for the support from the National Natural Science Foundation of China (51904077) and the Natural Science Foundation of Hebei Province (E2019203469).

## References

- 1 R. Vellacheri, A. Al-Haddad, H. Zhao, W. Wang, C. Wang and Y. Lei, High performance supercapacitor for efficient energy storage under extreme environmental temperatures, *Nano Energy*, 2014, **8**, 231–237.
- 2 A. S. Westover, J. W. Tian, S. Bemath, L. Oakes, R. Edwards, F. N. Shabab, S. Chatterjee, A. V. Anilkumar and C. L. Pint, A multifunctional load-bearing solid-state supercapacitor, *Nano Lett.*, 2014, **14**, 3197–3202.
- 3 J. Chmiola, C. Largeot, P. L. Taberna, P. Simon and Y. Gogotsi, Monolithic carbide-derived carbon films for micro-supercapacitors, *Science*, 2010, **328**, 480–483.
- 4 D. Pech, M. Brunet, H. Durou, P. Huang, V. Mochalin, Y. Gogotsi, P. L. Taberna and P. Simon, Ultrahigh-power micrometre-sized supercapacitors based on onion-like carbon, *Nat. Nanotechnol.*, 2010, **5**, 651–654.
- 5 J. Duay, S. A. Sherrill, Z. Gui, E. Gillette and S. B. Lee, Self-limiting electrodeposition of hierarchical MnO<sub>2</sub> and M(OH)<sub>2</sub>/MnO<sub>2</sub> nanofibril/nanowires: mechanism and supercapacitor properties, *ACS Nano*, 2013, **7**, 1200–1214.
- 6 A. K. Singh, D. Sarkar, G. G. Khan and K. Mandal, Hydrogenated NiO nanoblock architecture for high performance pseudocapacitor, *ACS Appl. Mater. Interfaces*, 2014, **6**, 4684–4692.
- 7 Y. Z. Su, K. Xiao, N. Li, Z. Q. Liu and S. Z. Qiao, Amorphous Ni(OH)<sub>2</sub>@ three-dimensional Ni core-shell nanostructures for high capacitance pseudocapacitors and asymmetric supercapacitors, *J. Mater. Chem. A*, 2014, **2**, 13845–13853.
- 8 K. Wang, H. Wu, Y. Meng and Z. Wei, Conducting polymer nanowire arrays for high performance supercapacitors, *Small*, 2014, **10**, 14–31.
- 9 G. F. Chen, Z. Q. Liu, J. M. Lin, N. Li and Y. Z. Su, Hierarchical polypyrrole based composites for high performance asymmetric supercapacitors, *J. Power Sources*, 2015, **283**, 484–493.
- 10 A. Ramadoss, K. N. Kang, H. J. Ahn, S. I. Kim, S. T. Ryu and J. H. Jang, Realization of high performance flexible wire supercapacitors based on 3-dimensional NiCo<sub>2</sub>O<sub>4</sub>/Ni fibers, *J. Mater. Chem. A*, 2016, **4**, 4718–4727.
- 11 J. W. Mao, C. H. He, J. Q. Qi, A. B. Zhang, Y. W. Sui, Y. Z. He, Q. K. Meng and F. X. Wei, An asymmetric supercapacitor with mesoporous NiCo<sub>2</sub>O<sub>4</sub> nanorod/graphene composite and N-doped graphene electrodes, *J. Electron. Mater.*, 2017, **47**, 512–520.
- 12 Z. Wu, Y. Zhu and X. Ji, NiCo<sub>2</sub>O<sub>4</sub>-based materials for electrochemical supercapacitors, *J. Mater. Chem. A*, 2014, **2**, 14759–14772.
- 13 H. Tong, S. Yue, F. Jin, L. Lu, Q. Meng and X. Zhang, Honeycomb-like NiCo<sub>2</sub>O<sub>4</sub>@Ni(OH)<sub>2</sub> supported on 3D N-doped graphene/carbon nanotubes sponge as an high performance electrode for supercapacitor, *Ceram. Int.*, 2017, **44**, 3113–3121.
- 14 Y. Sun, X. Xiao, P. Ni, Y. Shi, H. Dai, J. Hu, Y. Wang, Z. Li and Z. Li, DNA-templated synthesis of nickel cobaltite oxide nanoflake for high-performance electrochemical capacitors, *Electrochim. Acta*, 2014, **121**, 270–277.
- 15 L. Zhang, L. Dong, M. Li, P. Wang, J. Zhang and H. Lu, Ultrahigh-rate, ultralong-life asymmetric supercapacitors based on few-crystalline, porous NiCo<sub>2</sub>O<sub>4</sub> nanosheet composites, *J. Mater. Chem. A*, 2018, **6**, 1412–1422.





- 16 H. Jiang, J. Ma and C. Li, Hierarchical porous  $\text{NiCo}_2\text{O}_4$  nanowires for high-rate supercapacitors, *Chem. Commun.*, 2012, **48**, 4465–4467.
- 17 R. Zou, K. Xu, T. Wang, G. He, Q. Liu, X. Liu, Z. Zhang and J. Hu, Chain-like  $\text{NiCo}_2\text{O}_4$  nanowires with different exposed reactive planes for high-performance supercapacitor, *J. Mater. Chem. A*, 2013, **1**, 8560–8566.
- 18 E. Jökar, A. Irajizad and S. Shahrokhian, Synthesis and characterization of  $\text{NiCo}_2\text{O}_4$  nanorods for preparation of supercapacitor electrodes, *J. Solid State Electrochem.*, 2015, **19**, 269–274.
- 19 C. An, Y. Wang, Y. Huang, Y. Xu, C. Xu, L. Jiao and H. Yuan, Novel three-dimensional  $\text{NiCo}_2\text{O}_4$  hierarchitectures: solvothermal synthesis and electrochemical properties, *CrystEngComm*, 2014, **16**, 385–392.
- 20 Y. Zhu, X. Ji, R. Yin, Z. Hu, X. Qiu, Z. Wu and Y. Liu, Nanorod-assembled  $\text{NiCo}_2\text{O}_4$  hollow microspheres assisted by an ionic liquid as advanced electrode materials for supercapacitors, *RSC Adv.*, 2017, **7**, 11123–11128.
- 21 Y. Li, X. Hou, Z. Zhang, Z. Hai, H. Xu, D. Cui, S. Zhuykov and C. Xue,  $\text{NiCo}_2\text{O}_4$  particles with diamond-shaped hexahedron structure for high-performance supercapacitors, *Appl. Surf. Sci.*, 2018, **436**, 242–251.
- 22 W. Liu, C. Lu, K. Liang and B. K. Tay, A three dimensional vertically aligned multiwall carbon nanotube/ $\text{NiCo}_2\text{O}_4$  core/shell structure for novel high-performance supercapacitors, *J. Mater. Chem. A*, 2014, **2**, 5100–5107.
- 23 L. Wang, X. Jiao, P. Liu, Y. Ouyang, X. Xia, W. Lei and Q. Hao, Self-template synthesis of yolk-shelled  $\text{NiCo}_2\text{O}_4$  spheres for enhanced hybrid supercapacitors, *Appl. Surf. Sci.*, 2018, **427**, 174–181.
- 24 H. Chen, C. K. Hsieh, Y. Yang, X. Y. Liu, C. H. Lin, C. H. Tsai, Z. Q. Wen, F. Dong and Y. X. Zhang, Hierarchical nickel cobaltate-manganese dioxides core-shell nanowire arrays on graphene-decorated nickel foam for high-performance supercapacitors, *ChemElectroChem*, 2017, **4**, 2414–2422.
- 25 D. Cai, B. Liu, D. Wang, L. Wang, Y. Liu, R. Wang, Q. Li and T. Wang, Construction of unique  $\text{NiCo}_2\text{O}_4$  nanowire@ $\text{CoMoO}_4$  nanoplate core/shell arrays on Ni foam for high areal capacitance supercapacitors, *J. Mater. Chem. A*, 2014, **2**, 4954–4960.
- 26 H. Wang, C. M. B. Holt, Z. Li, X. Tan, B. S. Amirkhiz, Z. Xu, B. C. Olsen, T. Stephenson and D. Mitlin, Graphene-nickel cobaltite nanocomposite asymmetrical supercapacitor with commercial level mass loading, *Nano Res.*, 2012, **5**, 605–617.
- 27 M. J. Allen, V. C. Tung and R. B. Kaner, Honeycomb carbon: a review of graphene, *Chem. Rev.*, 2010, **110**, 132–145.
- 28 K. S. Novoselov, A. K. Geim, S. V. Morozov, D. Jiang, Y. Zhang, S. V. Dubonos, I. V. Grigorieva and A. A. Firsov, Electric field effect in atomically thin carbon films, *Science*, 2004, **306**, 666–669.
- 29 S. S. Jayaseelan, S. Radhakrishnan, B. Saravanakumar, M. K. Seo, M. S. Khil, H. Y. Kim and B. S. Kim, Mesoporous 3D  $\text{NiCo}_2\text{O}_4$ /MWCNT nanocomposite aerogels prepared by a supercritical  $\text{CO}_2$  drying method for high performance hybrid supercapacitor electrodes, *Colloids Surf., A*, 2018, **538**, 451–459.
- 30 C. Zhang, C. Lei, C. Cen, S. Tang, M. Deng, Y. Li and Y. Du, Interface polarization matters: enhancing supercapacitor performance of spinel  $\text{NiCo}_2\text{O}_4$  nanowires by reduced graphene oxide coating, *Electrochim. Acta*, 2018, **260**, 814–822.
- 31 H. Yang, C. Zeng, C. Sun, M. Wang and Y. Gao, Mesopores  $\text{NiCo}_2\text{O}_4$  nano-needles directly grown on Ni foam as high-performance electrodes for supercapacitors, *Mater. Lett.*, 2020, **279**, 128523.
- 32 Z. Wei, J. Guo, M. Qu, Z. Guo and H. Zhang, Honeycombed-like nanosheet array composite  $\text{NiCo}_2\text{O}_4$ /rGO for efficient methanol electrooxidation and supercapacitors, *Electrochim. Acta*, 2020, **362**, 137145.
- 33 N. I. Kovtyukhova, P. J. Ollivier, B. R. Martin, T. E. Mallouk, S. A. Chizhik, E. V. Buzaneva and A. D. Gorchinskiy, Layer-by-layer assembly of ultrathin composite films from micron-sized graphite oxide sheets and polycations, *Chem. Mater.*, 1999, **11**, 771–778.
- 34 X. Li, L. Jiang, C. Zhou, J. Liu and H. Zeng, Integrating large specific surface area and high conductivity in hydrogenated  $\text{NiCo}_2\text{O}_4$  double-shell hollow spheres to improve supercapacitors, *NPG Asia Mater.*, 2015, **7**(3), e165.
- 35 W. Zhang, W. Xin, T. Hu, Q. Gong, T. Gao and G. Zhou, One-step synthesis of  $\text{NiCo}_2\text{O}_4$  nanorods and firework-shaped microspheres formed with necklace-like structure for supercapacitor materials, *Ceram. Int.*, 2019, **45**(7), 8406–8413.
- 36 S. Sahoo and J. J. Shim, Facile synthesis of three-dimensional ternary  $\text{ZnCo}_2\text{O}_4$ /reduced graphene oxide/NiO composite film on nickel foam for next generation supercapacitor electrodes, *ACS Sustainable Chem. Eng.*, 2016, **5**, 241–251.
- 37 M. C. Biesinger, B. P. Payne, L. W. M. Lau, A. Gerson and R. S. C. Smart, X-ray photoelectron spectroscopic chemical state quantification of mixed nickel metal, oxide and hydroxide systems, *Surf. Interface Anal.*, 2009, **41**, 324–332.
- 38 L. Wang, X. Jiao, P. Liu, Y. Ouyang, X. Xia, W. Lei and Q. Hao, Self-template synthesis of yolk-shelled  $\text{NiCo}_2\text{O}_4$  spheres for enhanced hybrid supercapacitors, *Appl. Surf. Sci.*, 2018, **427**, 174–181.
- 39 Y. Changzhou, L. Jiaoyang, H. Linrui, Z. Xiaogang, S. Laifa and L. X. Wen, Ultrathin mesoporous  $\text{NiCo}_2\text{O}_4$  nanosheets supported on Ni foam as advanced electrodes for supercapacitors, *Adv. Funct. Mater.*, 2012, **22**, 4592–4597.
- 40 A. Lv, S. Lu, W. Xu, Z. Wang, Y. Shen and G. Liu, One-pot synthesis of  $\text{NiCo}_2\text{O}_4$ /rGO/NF hybrid electrode materials realizing ultrahigh capacitance and rapid charge/discharge at large current density, *Appl. Surf. Sci.*, 2020, **511**, 145538.
- 41 W. Zou, L. Zhang, L. Liu, X. Wang, J. Sun, S. Wu, Y. Deng, C. Tang, F. Gao and L. Dong, Engineering the  $\text{Cu}_2\text{O}$ -reduced graphene oxide interface to enhance photocatalytic degradation of organic pollutants under visible light, *Appl. Catal., B*, 2016, **181**, 495–503.
- 42 L. Zhang, D. Zhang, Z. Ren, M. Huo, G. Dang, F. Min, Q. Zhang and J. Xie, Mesoporous  $\text{NiCo}_2\text{O}_4$  micro/nanospheres with hierarchical structures for supercapacitors and methanol electrooxidation, *ChemElectroChem*, 2017, **4**, 441–449.



- 43 M. Ye, L. Ma, M. Gan, Y. Zhou, X. Li, F. Cao, F. Yan and Y. Zhai, One-step integration of the C/NiCo<sub>2</sub>O<sub>4</sub> mesoporous nanoneedle arrays on Ni foam for high-performance hybrid supercapacitors, *Appl. Surf. Sci.*, 2018, **456**, 390–397.
- 44 Z. Fan, J. Yan, T. Wei, L. Zhi, G. Ning, T. Li and F. Wei, Asymmetric supercapacitors based on graphene/MnO<sub>2</sub> and activated carbon nanofiber electrodes with high power and energy density, *Adv. Funct. Mater.*, 2011, **21**, 2366–2375.
- 45 A. Singh, S. K. Ojha and A. K. Ojha, Facile synthesis of porous nanostructures of NiCo<sub>2</sub>O<sub>4</sub> grown on rGO sheet for high performance supercapacitors, *Synth. Met.*, 2020, **259**, 116215.
- 46 D. R. Kumar, K. R. Prakasha, A. S. Prakash and J. J. Shim, Direct growth of honeycomb-like NiCo<sub>2</sub>O<sub>4</sub>@Ni foam electrode for pouch-type high-performance asymmetric supercapacitor, *J. Alloys Compd.*, 2020, **836**, 155370.
- 47 C. Huang, Y. Ding, C. Hao, S. Zhou, X. Wang, H. Gao, L. Zhu and J. Wu, PVP-assisted growth of Ni-Co oxide on N-doped reduced graphene oxide with enhanced pseudocapacitive behavior, *Chem. Eng. J.*, 2019, **378**, 122202.

